CO12-1 Research and Development of a High Counting Rate ^{3}He Position Sensitive Detector System

S. Satoh, K. Mori[1], Y. Yoshino[1], T. Seya, T. Otomo, H. Oshita, K. Okawa[2], N. Hikida[2], K. Ishizawa[2], A. Yamaguchi[3], M. Matsuura[3]

High Energy Accelerator Laboratory, KEK
[1] Institute for Integrated Radiation and Nuclear Science, Kyoto University
[2] Canon Electron Tubes & Devices Co., Ltd
[3] Clear-Pulse Co., Ltd

INTRODUCTION: Neutron scattering experiments are indispensable in the structural analysis of various forms of condensed matter and in the development of advanced materials. A ^{3}He gas detector [1], which is the most frequently used apparatus in the neutron experiments, is the best neutron detector available; however, the ^{3}He gas detector is low counting rate, less than 20 k cps (count per second).

In this research, we are developing to increase the counting rate of a ^{3}He gas position sensitive detector (PSD), and a maximum counting rate of 535 k cps has been obtained. Even if the usage range is approximately 200 k cps, the PSD with a high counting rate of 10 times that of an ordinary one has been completed.

EXPERIMENTS: At the B3 beam port in KUR at 5 MW operation on August 23, 2018, the counting rate of 535 k cps has been obtained. Since the neutron did not come out with uniform beam density, the counting rate was compared with a monitor counter.

RESULTS: Figure 1 shows the counting rate of the fast PSD versus the counting rate of the monitor counter. These data were obtained with the same condition. The usage range of the PSD is approximately 200 k cps, although the maximum counting rate is 535 k cps.

As shown in Fig. 2(a), a usual slow PSD which has a slow charge amplifier with a band-pass filter time constant 0.5 us generates the wide pulse width approximately 2 us. As shown in (b), a fast PSD which has a fast charge amplifier with a time constant of 0.05 us generates the narrow pulse width approximately 200 ns. If you use the slow PSD and the fast time constant amplifier, the PSD generates charge exceeding the time constant. Since the charge is differentiated before being sufficiently integrated, it becomes a low pulse height with wide pulse width. It has a risk of double counts or triple counts because of a charge fluctuation. Therefore, the fast circuit should not be used for the slow PSD.

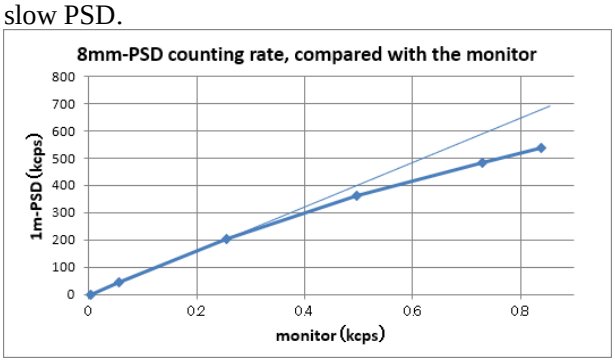

Fig. 1. Counting rate of the fast PSD, compared with the monitor counter.

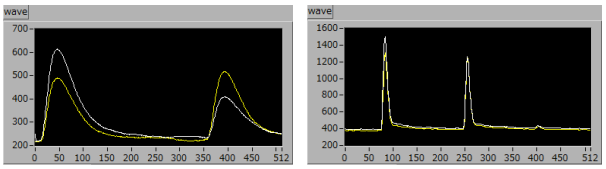

Fig. 2. (a) 0.5us amplifier for a slow PSD, (b) 0.05us amplifier for a fast PSD.

IMPROVEMENT: Since an ordinary PSD readout circuit is made to process the conventional slow PSDs, it is not suited for high counting rate. The following improvements have been added to the ordinary readout circuit to accommodate a high counting rate.

1- A fast time constant of charge amplifier has been developed for the fast PSD.

2- Data transmit way has been changed from bi-directional to uni-directional. G-bit network is also able to use and the maximum counting rate is able to be up to 300 k cps par PSD.

3- The fast PSD and slow PSD are able to be clearly distinguished by a pulse width measuring function that is installed in this version.

4- It is possible not to choose functions that inhibit the high counting rate.

REFERENCES:

[1] S. Satoh, S. Muto, N. Kaneko, T. Uchida, M. Tanaka, Y. Yasu, K. Nakayoshi, E. Inoue, H. Sendai, T. Nakatani, T. Otomo, Development of a readout system employing high-speed network for J-PARC, IPS08 Proc. Int. Symp. Pulsed Neutron Muon Sci. at J-PARC 2008, DOI:10.1016/j.nima.2008.11.054.

CO12-2 Dependency of Coherent Cherenkov Radiation Matched to the Circular Plane on Apex Angles of a Hollow Conical Dielectric

N. Sei and T. Takahashi[1]

Research Institute for Measurement and Analytical Instrumentation, National Institute of Advanced Industrial Science and Technology

[1]Institute for Integrated Radiation and Nuclear Science, Kyoto University

INTRODUCTION: To obtain intense terahertz (THz) waves, we proposed a principle of coherent Cherenkov radiation matched to the circular plane (CCR-MCP) [1]. We observed intense THz-wave radiation by using scheme of the CCR-MCP with an L-band linac at Kyoto University Institute for Integrated Radiation and Nuclear Science [2,3]. The radiation had the characteristics of the CCR-MCP, that is, the power of the radiation was proportional to the height of the hollow conical dielectric and a delay corresponding to the refractive index of the hollow conical dielectric was observed. To identify this radiation as the CCR-MCP, it was necessary to indicate that phase matching condition on the base of the hollow conical was satisfied when the apex angle of the hollow conical is half of the Cherenkov angle. Therefore, we investigated the dependency of the CCR-MCP on the apex angle.

EXPERIMENTS: High-density polyethylene (HDPE) was used as a material for the hollow conical dielectric. To prevent the electron beam from colliding with the hollow conical dielectric, the inner diameter of the hollow conical dielectric was set to be 16 mm. An aluminum collimator with an aperture diameter of 12 mm was installed in front of the hollow conical dielectric. Because the refractive index of the HDPE was 1.53 in the terahertz (THz) region, theoretical value of the apex angle satisfying the phase matching condition on the basal plane of the hollow conical dielectric was 24.6 degree. CCR beam generated in a hollow conical dielectric which did not satisfied the phase matching condition spread on a conical surface. It was difficult to transport the CCR beam without losing the power. Then, we have prepared hollow conical dielectrics with apex angles of 20 and 30 degrees in addition to the apex angle of 24.6 degree. Matching the effective length, at which the electron beam generated the CCR extracted on the basal plane, for each hollow conical dielectric, the heights of the hollow coni-cal dielectric were 60.4, 55, and 50 mm for the apex an-gles of 20, 24.6, and 30 degrees, respectively.

In the experiments, the electron energy was set to be 40 MeV and the electron-beam current was approxi-mately 0.18 mA. The duration and the repetition fre-quency were 22 ns and 30 Hz, respectively. The CCR was detected by a silicon bolometer and a Martin-Puplett in-terferometer with a step interval of 100 μm.

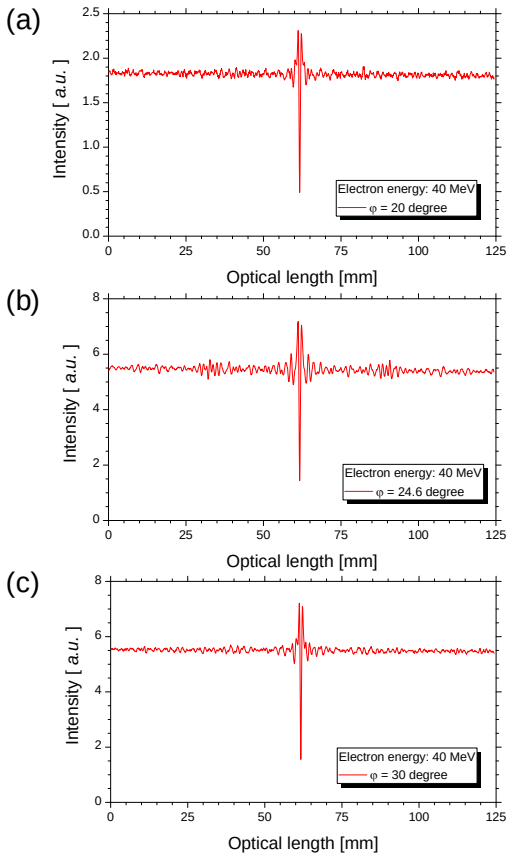

Fig. 1 Measured interferograms for the apex angles of (a) 20, (b) 24.6, and (c) 30 degrees.

RESULTS: Because the CCR passes through the dielectric, it delays the time to reach the detector compared to coherent diffraction radiation (CDR) generated at the exit of the aluminum collimator. As Fig. 1 shows, interference waveforms by the CCR and the CDR appeared at positions away from the center burst in the interferogram only when the apex angle was 24.6 mm. The distance between the interference waveform and the center burst is equal to the optical path difference between the CCR-MCP and the CDR considering the diffractive index of the HDPE. These experimental results demonstrate that the CCR-MCP can be observed only when the apex angle satisfies the phase matching condition. A series of experiments have shown that the theory of the CCR-MCP can describe the characteristics of the observed THz-waves. We plan to develop a high-power THz-wave source based on the principle of the CCR-MCP using high-quality electron beams in an advanced accelerator facility in the future.

REFERENCES:

[1] N. Sei *et al*., Phys. Lett. A **379** (2015) 2399.
[2] T. Takahashi *et al*., Phys. Rev. E **62** (2000) 8606.
[3] N. Sei and T. Takahashi, Sci. Rep. **7** (2017) 17440.

CO12-3 Neutron Activation Analysis for the stability monitoring of reference materials

T. Takatsuka, K. Hirata, Y. Iinuma[1], R. Okumura[1], and K. Takamiya[1]

National Metrology Institute of Japan, National Institute of Advanced Industrial Science and Technology
[1]Institute for Integrated Radiation and Nuclear Science, Kyoto University

INTRODUCTION: For high-performance silicon semiconductor devices, dopants are ion–implanted at lower energy to make shallower electric junctions. Dopant concentration should be controlled in 2 % as indicated in the international technology roadmap for semiconductors (ITRS) 2013 [1]. Several techniques, such as secondary ion mass spectrometry (SIMS) and Rutherford backscattering spectrometry (RBS), are widely used for characterizing the depth profiles of dopant concentration. In order to quantify the dopant concentration by these techniques, reference materials are required for calibration. Thus, certified reference materials (CRMs) of shallow arsenic implants in silicon were developed at the National Metrology Institute of Japan (NMIJ) [2].

This study aims to monitor arsenic quantity in the CRM by neutron activation analysis (NAA), and to confirm the reliability of the CRM.

EXPERIMENTS: For the fabrication of CRM, arsenic ions were implanted into Si(001) wafers at an energy of 10 keV and the nominal dose of 3×10^{15} /cm^2. The wafers were diced into 15 × 15 mm squares pieces by dicing saw. Several specimens were picked-up randomly at each time of the monitoring.

Arsenic amounts were evaluated by NAA with an internal standard method. For the production of standards to calibrate arsenic amounts, a working standard solution was prepared by diluting SRM 3103 (commercially available from NIST) gravimetrically. In addition, a standard solution for internal standard was prepared by diluting gold standard solution (SRM 3121) gravimetrically. A portion of the gold solution was dropped from a polyethylene pipette onto a cleaned filter paper on the CRM specimen. Portions of mixed solution (arsenic and gold standards) were dropped onto cleaned filter papers for the standards. All specimens and standards were heat-sealed in individual clean poly-ethylene envelopes and stacked in a poly-ethylene irradiation container. The neutron irradiation was performed for two hours with a 5.5×10^{12} cm^{-2}·s^{-1} thermal neutron fluence rate at Pn-2 in research reactor KUR of Institute for Integrated Radiation and Nuclear Science, Kyoto University. Gamma-ray activity of each specimen and standard was measured by a high-purity germanium detector (CANBERRA).

RESULTS: Figure 1 shows a gamma-ray spectrum obtained from the CRM specimen with gold internal standard solution. The peaks at around 559 keV from ^{76}As and 412 keV from ^{198}Au were focused to determine arsenic amount in the specimens. The counts in each peak were integrated for every specimen and standard, and then the intensities after the decay correction [3] were used to calculate relative intensities (^{76}As cps) / (^{198}Au cps/ ng). The arsenic content in the specimen is estimated from the calibration curve.

The monitoring results of arsenic area density are summarized in Fig. 2. The quantified values agree with each other on certification (●) and on monitoring (■), considering the uncertainties indicated with error bars. This shows the stability of the CRM for at least 8 years.

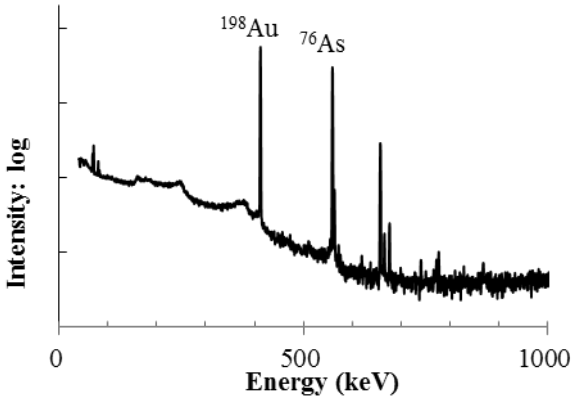

Fig. 1. Gamma-ray spectrum of the specimen with gold standard solution.

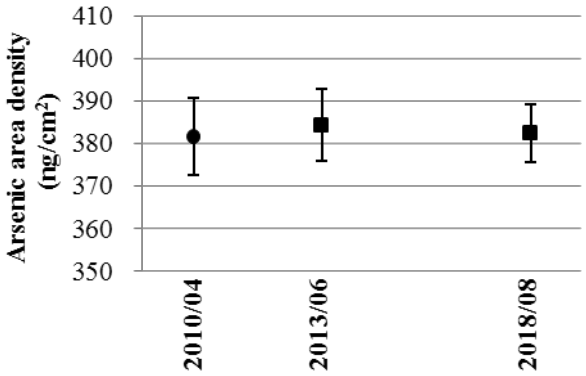

Fig. 2. The monitoring results of arsenic area density.

REFERENCES:

[1] International Technology Roadmap for Semiconductors 2013.
[2] Certificate of NMIJ-CRM 5603-a: Low energy arsenic implanted silicon, NMIJ / AIST.
[3] G.Gilmore and J. D. Hemingway, Practical gamma-ray spectrometry (John Wiley & Sons, Chichester, 1995.

CO12-4

Friction Reduction by the Combination Use of MoDTC and Organic Friction Modifier

T. Hirayama, N. Kikuchi[1], Y. Sasaki[1], M. Hino[2]

Dept. of Mechanical Eng., Doshisha University
[1]Dept. of Mechanical Eng., Graduate School of Doshisha University
[2]Institute for Integrated Radiation and Nuclear Science, Kyoto University

INTRODUCTION: Engine oil is a blend of base oil such as mineral oil and synthetic oil with additives, and it contributes to saving fuel by reducing the friction loss of the engine. Therefore, among various additives, those having a friction reducing effect under boundary lubricated conditions are blended in the engine oil, of which molybdenum dithiocarbamate (MoDTC) is particularly effective. MoDTC is known to produce a boundary lubrication layer containing molybdenum disulfide (MoS_2), which is effective for reducing friction. In addition, it is recently expected that a system using a combination organic friction modifier (OFM) that has no phosphorus in its molecule and MoDTC will alleviate environmental problems and obtain a sufficient friction reducing effect. The lubrication properties under boundary lubricated conditions are greatly influenced by the interfacial structure of the boundary lubrication layer formed by additives. Therefore, the interfacial structure formed by the combination use of MoDTC and OFM and its nanotribological properties were investigated in this study.

EXPERIMENTS: In this study, the oil in which MoDTC (0.3 mass%) and OFM is added to the base oil was used as the lubricating oil model. Hexadecane and palmitic acid (0.1 mass%) were used as models for the base oil and OFM. For neutron reflectometry (NR), deuterated palmitic acid, was used for the purpose of facilitating the analysis since a clear difference occurs in the reflectivity profile between hydrogen and deuterium.

We used the time-of-flight (TOF) type neutron reflectometer SOFIA installed at the J-PARC in Tokai, Ibaraki. In order to grasp the film thickness and density of the boundary lubrication layer formed on the Cu surface under each system added alone or in combination, experiments were conducted to obtain the reflectivity profile under each case.

RESULTS: First, we conducted the NR experiment to investigate the boundary layer structure formed by *d*-palmitic acid. When *d*-palmitic acid was added, the fringe interval became short; as a result of the analysis, it was found that an adsorption layer having a thickness of about 2.1 nm was formed on the copper surface immediately after the addition of *d*-palmitic acid. The SLD value of *d*-palmitic acid at the bulk state was 6.7×10^{-6} Å^{-2}, whereas the analysis value was 2.1×10^{-6} Å^{-2}. From this, the density of the adsorption layer was approximately 30% with respect to the bulk density. From 0h to 2h, the fringe interval did not change; it indicated that the film thickness and the density of the adsorption layer by *d*-palmitic acid barely change with time.

For the combined system being used, measurements were carried out under the three cases described below. [Case 1]: Measurement was carried out for four hours after placing hexadecane+*d*-palmitic acid (0.1 mass%) + MoDTC (0.3 mass%) into the sample holder. [Case 2]: Measurement was carried out for two hours after hexadecane+*d*-palmitic acid (0.1 mass%) was placed in the sample holder. After the measurement, the sample holder was rinsed with hexadecane, and hexadecane+ MoDTC (0.3 mass%) was added, and then the measurement was carried out for four hours. [Case 3]: Measurement was carried out for four hours after hexadecane+MoDTC (0.3 mass%) was placed in the sample holder. After the measurement, the sample holder was rinsed with hexadecane, and hexadecane+*d*-palmitic acid (0.1 mass%) was added, and then the measurement was carried out for two hours.

As a result of analysis of [Case 1], it was found that an adsorption layer with a thickness of about 2 nm and a density of approximately 30% with respect to the bulk density was formed immediately after *d*-palmitic acid was added. Although the film thickness did not change with time, the density increased to about 60% in four hours. When MoDTC is added first, film thickness and density cannot be detected since MoDTC was not deuterated. However, from the NR experiment of [Case 3], it can be seen that immediately after the addition of *d*-palmitic acid, an adsorption layer having the 2-nm film thickness and the approximately 30% density with respect to the bulk density is formed. While no change in film thickness with time was observed, the density increased from about 30% to about 45% in 2 hours. This result is shows the same tendency with as [Case 1]. In addition, it is interesting to note that the nanotribological property measured by SiO_2 colloidal probe was better when we used MoDTC and palmitic acid in combination than that when we used only MoDTC or palmitic acid each. It indicated that the combination use of MoDTC and OFM is effective for friction reduction by forming thicker boundary lubrication layer.

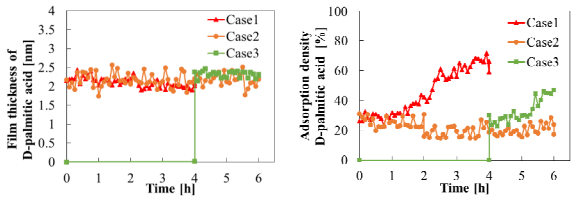

Fig. 1. Estimated film thickness and density of palmitic acid by neutron reflectometry for the three cases.

CO12-5 Strutctural studies of water-solubule menaquinone-7 from *Bacillus subtilis natto*

T. Chatake, T. Saito, K. Morishima, R. Inoue, M. Sugiyama, T. Kikkou[1], O. Matsumoto[1], R.Takayama[1], Y. Yanagisawa[1]
Institute for Integrated Radiation and Nuclear Science, Kyoto University
[1]Faculty of Pharmacy, Chiba Institute of Science.

INTRODUCTION: Natto is a popular fermented food in Japan. In manufacturing process of natto, *Bacillus subtilis natto* (BSN) produces various biologically active substances, which contribute to health. Especially, this bacterium produces a large quantity of menaquinone-7 (MK-7), which is a kind of vitamin K that contribute to osteogenesis [1] and blood coagulation [2]. While MK-7 is a fat-soluble compound, BSN produces a water-soluble complex of MK-7 (*natto*-MK-7) [3,4]. This property is the attractive point in application uses of *natto*-MK-7. Previously, it was reported that the size of *natto*-MK-7 was estimated to be ~100 kDa by size-exclusion chromatography [3,4], and that small peptides with the size of ~3 kDa (called K-binding factor in [4]) in *natto*-MK-7 contribute to water solubilization of MK-7 [4]. However, the further structural information had not been reported after reports of Ikeda and Doi [4]. The aim of our study is to reveal the structural mechanism of the water solubilization of *natto*-MK-7. Last year, we reported the established protocol of the purification and preliminary structural analysis *natto*-MK-7 [5]. In the present study, we further refined the purification protocol of *natto*-MK-7 and performed various analyses using highly purified *natto*-MK-7.

EXPERIMENTS: *Bacillus subtilis natto* (miyagino strain) was cultured in liquid medium, and the cultured medium was concentrated to 24 mL. 21 mL of the 24 mL was used for purification. Purification was carried out by a series of fast protein liquid chromatography (FPLC). The first FPLC was an ion exchange chromatography using the couple of DEAE sepharose FF with the column volume (CV) of 5 mL. The coupled columns (CV = 10 mL) were equilibrated by 20 mM Tris-HCl and 0.3 M NaCl buffer. Prior to injection, the salt concentration of the sample solution was adjusted by adding 9 mL of 1 M NaCl buffer solution (20 mM Tris-HCl (pH7.6)), then the sample solution was directly injected to the coupled column to avoid any damage on FPLC system. After the injection, the column was connected to the FPLC system. After 5 CV wash by 20 mM Tris-HCl and 0.3 M NaCl buffer, *natto*-MK-7 was eluted from the column by the gradient elution method, where NaCl concentration was gradually increased from 0.3 M to 1.0M during 10 CV. The second and third chromatography were carried out using another couple of DEAE sepharose FF columns. Before each injection, the NaCl concentration of the *natto*-MK-7 solution was adjusted to be below 0.3 M by adding the same volume of 20 mM Tris-HCl buffer (pH7.5). Wash and gradient protocols were same as the first chromatography. The final purification was performed by size-exclusion chromatography using GE Hiprep 16/60 sephacryl S-300. 2.5 mL of the eluted natto-MK-7 solution was injected to the column, and the chromatography was carried out with the rate of 0.4 mL/min using 20 mM Tris-HCl buffer (pH7.6) containing 0.1 M NaCl. Confirmation of the presence of *natto*-MK-7 was done by measuring MK-7 activity of each fraction eluted from the size-exclusion chromatography. The fraction was processed with hexane and analyzed by the high-performance liquid chromatography as reported previously [3,6].

RESULTS: In chromatography charts in the first and second FPLC, the elution curves of natto-MK-7 were not symmetrical, and MK-7 activities were observed in the fractions of the wash process while the activity was hardly observed in the second and third wash process. These results suggested the presence of the other structural type of *natto*-MK-7 than the purified *natto*-MK-7 in this experiment, although the present purified *natto*-MK-7 is the main product of *Bacillus subtilis natto*. ~11% of highly-purified *natto*-MK-7 could be obtained from the concentrated cultured medium by three times ion-exchange chromatography. Moreover, the *natto*-MK-7 has different sizes. In the final purification step by the size exclusion chromatography, large particles were observed as shown in Fig. 1. The activity of MK-7 were also confirmed in them, suggesting that the *natto*-MK-7 naturally aggregate. These structures were investigated by dynamic light scattering (DLS), analytical centrifugation (AUC) in IRNS, and atomic force microscopy (AFM) in Chiba institute of science. The further discussion is in progress.

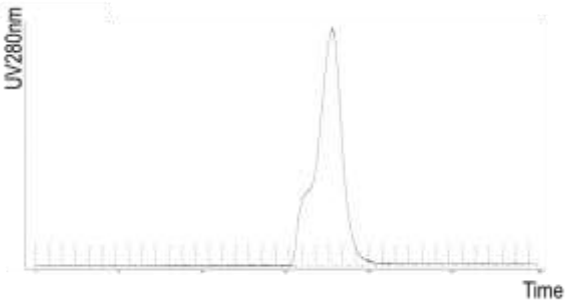

Fig. 1. The chart of the size-exclusion chromatography

REFERENCES:

[1] P.V. Hauschka, J.B. Lian, P. M. Gallop, Proc. Nat. Acad. Sci. USA **72** (1975) 3925–3929.
[2] H. Dam, Biochem. J. **29** (1935) 1273–1285.
[3] H. Sumi et *al.*, Clinical Pharmacology and Therapy **18** (2008) 297–305.
[4] H. Ikeda, Y. Doi, Y. Eur. J. Biochem. **192** (1990) 219–224.
[5] T. Chatake *et al.*, J. Food. Biochem. **42** (2018) e12630.
[6] Y. Yanagisawa, H. Sumi, H. J. Food. Biochem. **29** (2005) 267–277.

CO12-6 Neutron Activation Analysis of Cultivated Oysters in Miyagi Prefecture

M. Fukushima[1], A. Chatt[2], Y. Iinuma[3] and T. Maeda[1]

[1]*Department of Food and Environment, Ishinomaki Senshu University*

[2]*Department of Chemistry, Dalhousie University*
[3]*KURNS, Kyoto University*

INTRODUCTION: Miyagi Prefecture is the second largest producer of cultivated oysters in Japan, and most of the cultivated bays are located in northern part of Miyagi. Mating season of oysters in Miyagi Pref. is July-August due to preferred sea water temperature. Weight of soft tissues of oysters changes drastically before and after the mating season. No data are available on the element levels of oysters before and after the mating season. Selected trace element levels of soft tissues before and after the mating season were analyzed using neutron activation analysis (NAA). Bioaccesible fraction of trace elements in soft tissues of oysters was also estimated to investigate any seasonal variation. We have collected cultivated oysters from seven different bays in Dec. 2003 – Oct. 2005 and analyzed trace elements. Geological and marine environment in Pacific side of Tohoku district have drastically changed by earthquake and tsunami in 3.11, 2011. We have collected cultivated oysters from seven different bays in Miyagi, and analyzed trace elements to compare the effect of earthquake and tsunami.

EXPERIMENTS: 1) Samples: Oysters, estimated birth month were July 2012 and 2013, were collected from Higashimatsushima, Miyagi every month between April to September in 2014. Soft tissues of each 5 oysters were separated from their shells, separated to hepatopancreas, muscle, gill, and mantle, freeze dried, and pulverized. Another group of oysters were collected from Tanoura, Shizugawa, Nagatsurahama, Ogatsu, Ohishihama, Obuchi, and Higashimatsushima in Miyagi in May 2015. Soft tissues were treated same way as written above.
2) Analysis of Bioaccesible Levels of Elements in Oyster Tissue: One gram of soft tissue (dried powder) was incubated for 15 min at 95℃ with 0.10 ml of α-Amilase, 30 min at 60℃ with 0.10 ml of 50 mg/ml Protease, then 30 min at 60℃ with 0.10 ml of Amyloglucosidate. Precipitate was filtered after adding ethyl alcohol, freeze dried, and pulverized.
3) NAA: Samples were irradiated in KUR for 1 min in TcPn, and measured gamma spectra for 5 min after 1.5 min decay, or 1 hr in Pn and measured for 30 min after 1 month decay.

RESULTS: 1) Sample weight: Average weight of soft tissues were 2.8, 6.2, 6.8, 2.6, 3.5, 6.0, 15.2, 26.4, 42.2, 6.8, 25.1, and 33.3 g (wet weight) for 10-15 and 21-26 months after the birth, respectively. Both of 2.6 g and 6.8 g were obtained for oysters collected July 2014 and the reason of the decrease might be the mating season.
2) Seasonal variation of elements: Zn, Fe, Ag, Se, and Sc showed peak in July for the seasonal variations of elemental levels in hepatopancreas of oysters. Example for Zn is shown in Fig. 1. Zn level showed peak in July, but the mass showed peak in June and it decreased in July.
3) Bioaccesible fraction of elements: Bioaccesible levels of Zn, Fe, Ag, and Sc were almost proportional to total levels in soft tissues. Example for Zn is shown in Fig. 2. Both of 12 and 25 months were July, and both of total and bioaccesible levels showed peaks in 12 and 25 months.
4) Locational Variation of element levels in oysters: When we have analyzed oysters collected in 2003-2005, all the elements analyzed showed lowest levels in hepatopancreas, mantle, gill, and muscle from Nagatsurahama. In this work, all the element levels in organs from Nagatsurahama showed same levels as other 6 bays. In seven bays, geological condition of Nagatsurahama has changed most compared other six bays.

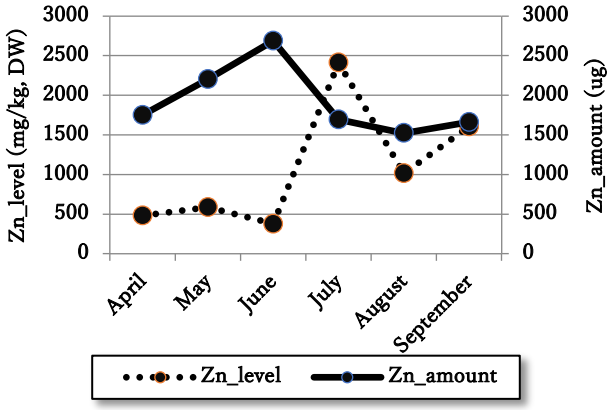

Fig. 1 Relation ships between Zn level and amount in hepatopancreas of seasonal variation.

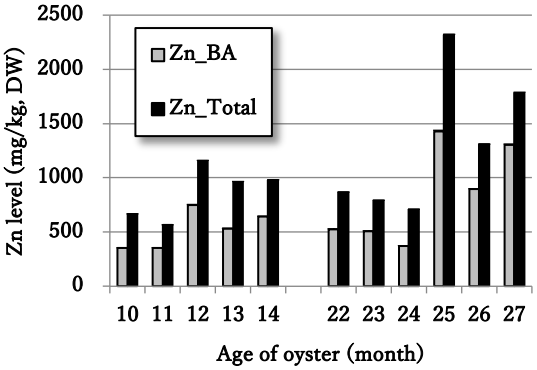

Fig. 2 Seasonal variations of total and bioaccesible levels in soft tissues.

Acknowledgement: We thank to Mr. Watanabes and Marine Technology Center of Miyagi Prefecture for supplying oyster samples for us. We also thank to Dr. Takeshige Matsutani in Ishinomaki Senshu University for discussion with us.

CO12-7 **Monuments of contaminated objects and memories**
Nagadoro Area, Iitate Village, Fukushima

M. Takagaki
Neurosurgery, Louis Pasteur Center for Medical Research
Graduate School of Human and Environmental Study, Kyoto University

I participated in a field research of a media that covers temporary returning home of villagers in Iidate Village, Fukushima, which is still a restricted area for their highly radioactive area (photo. 1). Mr. and Mrs. K. have engaged in cutting out the abundant granite in the area, and took over the business of forming tombstones, etc. until the time of the earthquake after their marriage. Their daily living have been still forced to a refuge because of highly contaminated radioactive areas, but even the aging population, the intention to return to the village has been fading out. In this time, I will report my joint research with the media in victim's temporary returning home.


Photo 1

It was as if time had stopped in the house after the earthquake. Calendar shows March 2011. The radioactivity in front of the home entrance exceed 30 μSv / hr.

Mrs. K's narrative:

Mrs. K, do you still have a mind to come home to live here?

"No, I'm not ready to go home because I came to my daughter-in-law to this home and I don't stick to my home. It's already difficult to put in the artificial joints of my knee last month, and it's already past a year."

"Hmm, this is my room, I want to know the current radiation activity here." (Mrs. K does not get out from her room to join the media group, she does not move away from her own room.)
Mrs. K's room faces the back yard mountain and the radiation is relatively high even in the room.

"I eager to know about the radioactivity of my photos and Kimonos that is a memory of my young era."

"OK. I'll tell the media to come to measure their radiation activity. And they immediately said to Mrs. K that your items did not polluted."

"Oh-good, the photos is not radioactive, you can bring them back to your home"

"Congratulations!"

"Kimono is also good?, ... (while showing a picture of Japanese dance in a kimono, ...)"

It's also good!

"Oh, I feel bliss."


Photo 2

After that, Mrs. K always carried the photo album with her during stay in the field (Photo 2).

Although we can give up on things, the monuments of memory cannot be erased. Mrs. K must have realized a disaster recovery by recovering her album. The figures measured in the field were not just physical quantities, but, for Mrs. K, the figures themselves must have been her recovered memories themselves that were not polluted. Disaster recovery may be to arrange memory on the line to the future and recover one's life by means of material recovery from the dark spots.

To see a world in a grain of sand.
And a heaven in a wild flower, Hold infinity
in the palm of your hand.
And eternity in an hour. *By William Blake*

Acknowledgment: This study has been financially supported by National Research Fund No. 17Ki8536 2017-19 from the Ministry of Education, Culture, Sports, Science and Technology, Japan.

30045

CO12-8 Development of neutron imager based on hole-type MPGD with glass capillary plate

F. Tokanai[1], R. Itoh[2], T. Moriya[1], T. Sumiyoshi[3], H. Kondo[4], H. Sugiyama[4], M. Hayashi[4], T. Okada[4], M. Hino[5]

[1]*Faculty of Science, Yamagata University*
[2]*Graduate School of Science and Engineering, Yamagata University*
[3]*Graduate School of Science, Tokyo Metropolitan University*
[4]*Electron Tube Division, Hamamatsu Photonics K. K.*
[5] *Institute for Integrated Radiation and Nuclear Science, Kyoto University*

INTRODUCTION: Neutron imaging is useful for light elements in the sample such as hydrogen, lithium, boron, carbon, and nitrogen. Owing to their unique ability to probe inside samples, neutrons have been widely utilized for neutron radiography in various fields, including fundamental science, archaeology, and industry.

High position resolution with a moderate effective area is required in practical applications of neutron imaging. We have been developing a high-spatial-resolution neutron gas scintillation imager (n-GSI) with a capillary plate gas detector (CPGD) [1]. Fig. 1 shows the operating principle of the CPGD. The detector consists of a conversion layer containing ^{10}B and a CP placed in a vessel. The vessel is filled with neon or argon gas mixtures. A ^{10}B converter is directly mounted on the inlet surface of the CP. Charged particles (α-rays and ^{7}Li nuclei) are generated by a nuclear reaction between incident neutrons and the ^{10}B. Since the ^{10}B converter is directly mounted on the inlet surface of the CP, the track length of the charged particles is restricted to within the capillary. Thus, the spatial resolution of incident neutrons is expected to be close to the capillary diameter.

The performance of the n-GSI was investigated using the cold neutron beam line CN-3 installed to the Kyoto University Reactor (KUR).

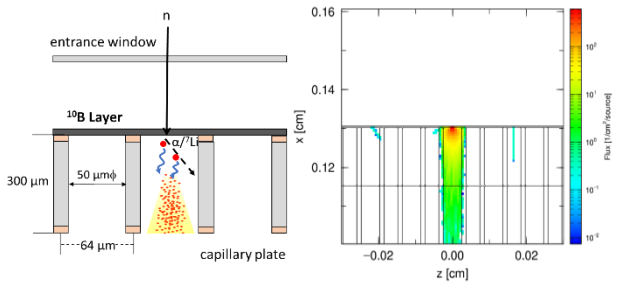

Fig. 1. Principle of the n-GSI and result of simulation using PHITS code [2].

EXPERIMENTS: Fig. 2 shows the experimental setup of the n-GSI. It consists of a CPGD filled with Ne (90%) and CF_4 (10%) gas mixture at 1 atm, mirror and lens optics, an image amplifier unit, and a cooled CMOS camera system. The CPGD consists of a converter layer and a CP in a sealed-type vessel [3]. The converter consists of a 2-μm-thick B_4C layer on a silicon substrate [4]. The converter is directly mounted on the CP. The CP has an effective diameter of 27 mm and a thickness, individual hole diameter, and pitch of 300 μm, 50 μm, and 64 μm, respectively. The neutron wavelength giving the maximum intensity and the total flux of the CN-3 guide tube were 2 Å and 3.8 × 10^6 neutron cm^{-2} s^{-1}, respectively. The n-GSI system was placed 300 mm from the downstream exit of the neutron guide. The neutrons were irradiated into a sample.

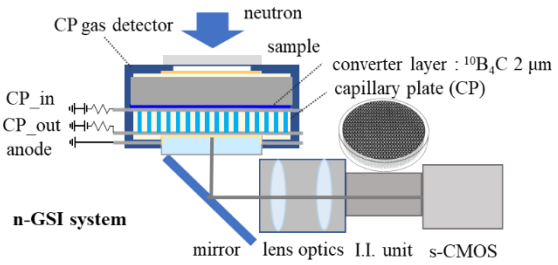

Fig. 2. Schematic view of n-GSI and experimental arrangement for evaluating performance using neutron beams from KUR.

RESULTS: Fig. 3 shows a neutron transmission image of a photomultiplier tube (PMT; Hamamatsu R9875) obtained using the n-GSI system [5]. The exposure time was 300 s. The structure of the dynode in the PMT is clearly seen in this image. Moreover, it is recognized that the neutrons are highly absorbed in the borosilicate glass compared with synthetic silica. This is because the borosilicate glass contains a large amount of boron, and hence the isotope of ^{10}B, as the main glass constituent.

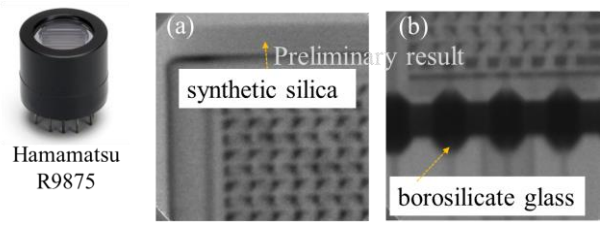

Fig. 3. Neutron transmission image of a photomultiplier tube (Hamamatsu R9875) obtained using the n-GSI system.

REFERENCES:

[1] T. Sumiyoshi *et al.,* Hamon 27 (1) (2017) 16-19.
[2] T. Sato *et al.,* J. Nucl. Sci. Technol. 55 (2018) 684.
[3] H. Kondo *et al.,* Plasma Fusion Res. 13 (2018) 2406018.
[4] M. Hino *et al.,* Nucl. Instrum. and Methods. A 797 (2015) 265.
[5] H. Kondo *et al.,* VCI 2019 conference.

CO12-9 Radius of Gyration of Polymer for Viscosity Index Improver at Various Temperatures Evaluated by Small-Angle X-Ray Scattering

T. Hirayama, R. Takahashi[1], K. Tamura[2], N. Sato[3], M. Sugiyama[3], M. Hino[3], Y. Oba[4]

Dept. of Mechanical Eng., Doshisha University
[1]Dept. of Mechanical Eng., Graduate School of Doshisha University
[2] Idemitsu Kosan Co., Ltd.
[3]Institute for Integrated Radiation and Nuclear Science, Kyoto University
[4]Japan Atomic Energy Agency

INTRODUCTION: Lubricating oils are necessary for friction reduction and high wear durability of sliding surfaces in machine components, and the development of the best oils is strongly required from industry. Viscosity index improver (VII) is a kind of additives for relieving the reduction of viscosity of lubricating oil due to temperature rise. Classical textbooks say that the VII molecules work with changing their equivalent radius in base oil in accordance with oil temperature. However, there are only few papers investigating the equivalent radius of VII molecules by small-angle X-ray scattering (SAXS) and/or small-angle neutron scattering (SANS)[1], and there is still room for discussion of the behavior and working mechanism of VII molecules in oil. This study tried to investigate the radius of gyration of several kinds of VII polymers in base oil at various temperatures by SAXS, and the behavior of polymers was investigated and discussed.

EXPERIMENT: To investigate the radius of gyration of VII polymer, we used a SAXS instrument (NANOPIX, Rigaku) with a Cu-target X-ray source emitting X-ray with a wavelength of 1.54 Å, a characteristic line of Cu-Kα. The 1.2 mm-thick aluminum cell having optical windows made of 20-μm thermally-resistant engineering plastic film (Superio-UT, Mitsubishi chemical) was used for the measurement. The cell temperature increased to be 25, 40, 60, 80 and 100ºC in turn, and the last measurement was carried out at 25ºC again after cooling for checking if the VII molecule degenerated or not by heat. Poly(methyl acrylate) (PMA) type VII, as shown in Fig. 1, was prepared as a typical one used in engine oil in the study. Squalane was used as a model base oil, and the concentrations of PMA into squalane were 0.5, 1.0 and 2.0 mass%.

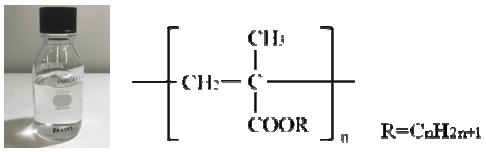

Fig. 1. Chemical structure of PMA type VII.

RESULTS AND DISCUSSION: The SAXS intensity profiles versus scattering vector q from squalane with 0.5 mass%-PMA type VII at each temperature were shown in Fig. 1, for example. The profiles were obtained by subtracting the intensity profiles from pure squalane at each temperature previously measured with the same liquid cell. The radius of gyration R_g and absolute intensity at the origin I_0 estimated from the Guinier plot are shown in Fig. 2. We can see that the intensity profiles had little change even if the temperature changed, and therefore the estimated R_g was almost constant in the observed range regardless of temperature rise. This result contradicts the fact that the PMA effectively work as VII. Meanwhile, it is interesting to note that I_0 gradually decreased in accordance with temperature rise. These facts indicate that the side chains of PMA molecules swell and expand in the squalane when the temperature rises, and then the core size of molecules estimated as R_g are almost constant while the I_0 decreased because the apparent atomic density for X-ray scattering decreased because of the side chain swelling in squalane. SANS will be tried to confirm the validity of this prediction as a next step.

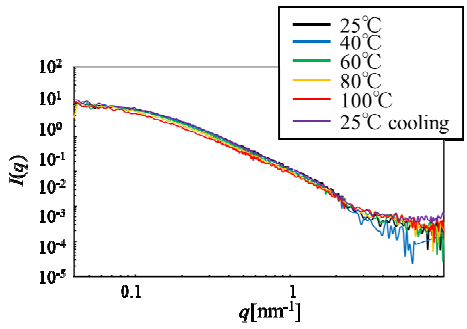

Fig. 1. SAXS profiles from squalane with 0.5 mass%-PMA type VII at various temperatures.

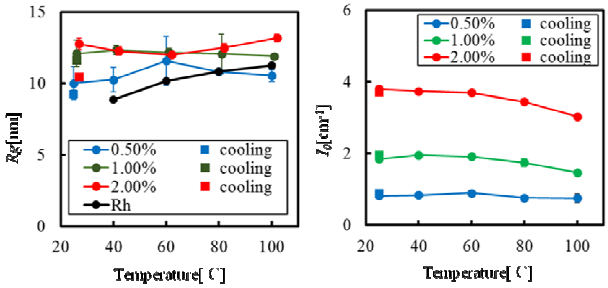

Fig. 2. Estimated Rg and I0 from Guinier plot of squalane with PMA type VII with various concentrations.

REFERENCES:

[1] M. J. Covitch, K. J. Trickett, How Polymers Behave as Viscosity Index Improvers in Lubricating Oils, Adv. Chem. Eng. Sci., 5 (2015) 134.

CO12-10 Study of Isotope Separation via Chemical Exchange Reaction

R. Hazama, T. Yoshimoto, Y. Sakuma[1], T. Fujii[2], T. Fukutani[3], Y. Shibahara[3]

Graduate School of Human Environment, Osaka Sangyo University
[1]Laboratory for Advanced Nuclear Energy, Tokyo Institute of Technology,
[2]Graduate School of Engineering, Osaka University
[3]Institute for Integrated Radiation and Nuclear Science, Kyoto University

INTRODUCTION: A liquid microspace formed by simple introduction of organic and aqueous phases into microchannel provides unique features of short molecular diffusion distance (T) and large specific interfacial area (S/V), which gives a fast and high conversion than that given by strong stirring and the other conditions for any macroscale reactions: S/V=200 & T=0.1s for 100μm [1].

EXPERIMENTS: Isotopic enrichment occurs according to the following chemical exchange reaction:

$$^{40}Ca^{2+}_{(aq)} + {}^{48}CaL^{2+}_{(org)} \rightarrow {}^{48}Ca^{2+}_{(aq)} + {}^{40}CaL^{2+}_{(org)} \quad (1)$$

where L represents macrocyclic polyether(18-crown-6). An aqueous solution (3M $CaCl_2$) and organic solution (0.7M DC18C6 in chloroform) were stirred by a single Y type microchip with 40 mm junction length (Fig. 2) at room temperature and separated. A stable liquid-liquid interface (Fig. 3) was formed by the introduction through two inlets of the microchip by microfluidic flow controller (Fig. 1). The output volume of one mL can be obtained by 30μl/min flow-rate for about 30 min.

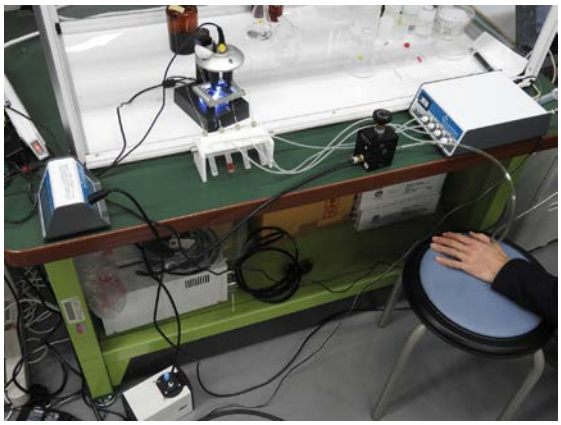

Fig 1. Photographs showing fast and high conversion phase-transfer tabletop system exploiting the liquid-liquid interface formed in a glass microchannel chip on microscope, microfluidic flow controller (MFCS-EZ), flow-rate sensors and air compressor of 0.7MPa.

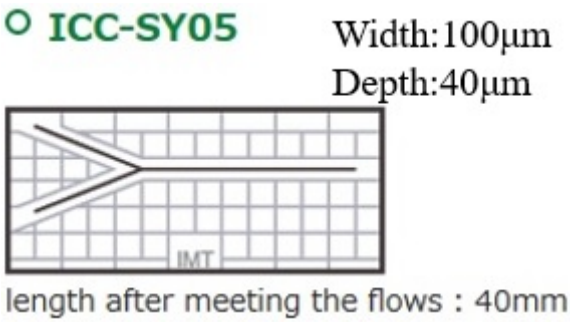

Fig 2. Single Y type microchip (ICC-SY05) with microchannel 100 μm wide, 40 μm deep and 4 cm length provided by IMT(Institute of Microchemical Technology Co., Ltd), which is made of borosilicate glass.

Fig 3. Laminar flow was formed by two solvents of aqueous(Right)-organic(Left) multiphase flow.

RESULTS: The Ca concentration in aqueous and organic phase for the laminar-flow was measured by ICP-MS. We obtained a similar value of about 20 % partition factor with the batch LLE process [2] and its Ca transfer between two phases without any stirring for only 0.3 sec (6000 times faster than [2]) on a chip, shown in Fig. 4.

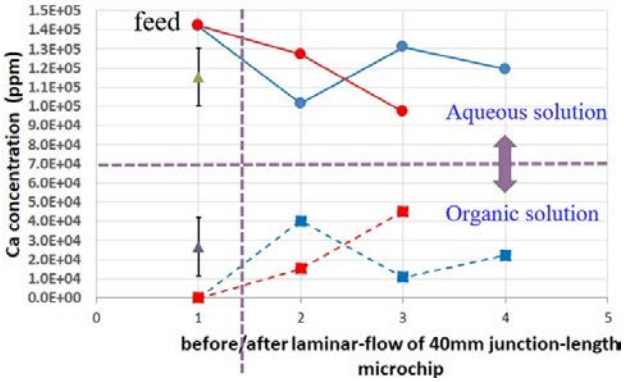

Fig 4. Ca concentration in aqueous phase (circle) and organic phase (square) for the laminar-flow of 4cm junction-length microchip. Triangle with error bar is the average of 2 – 4 after the reaction, 1 is feed solution for $CaCl_2$ aqueous and crown-ether organic ($CHCl_3$) phase.

REFERENCES:

[1]H. Hisamoto *et al.*, Chem. Commun. (2001) 2662.
[2]R. Hazama *et al.*, KURRI Progress Report 2017, 104.

CO12-11 Instrumental Neutron Activation Analysis of Iridium in a Chemical Reagent

T. Miura[1], R. Okumura[2], Y. Iinuma[2], S. Sekimoto[2], K. Takamiya[2]

[1]*National Metrology Institute of Japan, AIST*
[2] *Institute for Integrated Radiation and Nuclear Science, Kyoto University*

INTRODUCTION: National Metrology Institute of Japan (NMIJ) is responsible for developing certified reference materials and for establishing the traceability of SI (The International System of Units) on chemical metrology in Japan. To establish SI traceability, the primary method of measurements should be applied to the characterization of the certified reference materials. Recently, neutron activation analysis using comparator standard is recognized as a potential primary ratio method [1]. Despite the potential of neutron activation analysis as primary ratio method, the evaluation of the measurement uncertainty is required in any analysis. In general, there are three main components of uncertainty in neutron activation analysis, that is, sample preparation uncertainty, neutron flux homogeneity, and gamma ray measurement uncertainty. Usually, flux monitor is used to correct the neutron flux in-homogeneity. However, although the flux monitor can correct the neutron flux variation using the count rate of the known amount of the monitor nuclide, it does not reflect the neutron flux of the actual sample. The most practical method to eliminate neutron flux in-homogeneity and to improve gamma ray measurement uncertainty is an internal standard method [2-4]. For the development of primary inorganic standard solution as national standard, the purity of starting material has to be determined. The purity of starting material has to be determined for the development of primary inorganic standard solution as national primary standard. Recently, the needs of development the primary standard solution of precious metal including Rh, Pd, Ir, Os and Pt is increased from Japanese industry. However, it is well known that dissolution of high purity Iridium metal as most difficult case. And so, the purity of Iridium reagent an easy dissolution form was verified using instrumental neutron activation analysis. In this study, we presented that capability of instrumental neutron activation analysis for determination of Ir in high purity Iridium(IV) Bromide ($IrBr_4$).

EXPERIMENTS: The high purity $IrBr_4$ was purchased from Alfa Aesar. The informative purity value of the $IrBr_4$ was 99.99 % (metal basis). The comparator standard of Ir prepared from High purity Ir metal (Alpha Aesar, powder form, informative purity value was 99.99 % as metal basis). The Au solution for the internal standard was prepared from a high purity metal. The mass fraction of Au solution was 35 mg g^{-1}.

Few mill grams of $IrBr_4$ were weighed using Mettler Toledo XP26 micro balance. After adding the Au solution as internal standard, the samples of $IrBr_4$ in the polyethylene bags were heat sealed. The neutron irradiation was performed using KUR TCPn (thermal neutron flux: 8.0×10^{10} cm^{-2} s^{-1}) for 10min. The irradiated samples were cooled at 3 hours. The gamma rays from irradiated samples were measured using Canberra GC4070-7500 Ge detector with Laboratory Equipment Corporation MCA600. The measured radioactive isotopes were ^{192}Ir (γ ray energy; 316 keV and 468 keV, half-life; 73.829 day), ^{194}Ir (γ ray energy; 328 keV, half-life; 19.28 h) and ^{198}Au (γ ray energy; 412 keV, half-life; 2.6941 day) as internal standard).

RESULTS: In this study, Iridium in the high purity $IrBr_4$ sample could be precisely determined by instrumental neutron activation analysis with internal standard. The analytical results were shown in the Table 1. The improvement of linearity of calibration curves and measurement repeatability was successfully demonstrated by using the internal standard.

Table 1 Analytical results of Ir in $IrBr_4$

Nuclide	Measured γ ray	Mass fraction of Ir
^{192}Ir	316 keV	37.32 %
^{192}Ir	468 keV	37.47 %
^{194}Ir	328 keV	37.52 %
Mean ± RSD*		37.4 %±0.28 %

*relative standard deviation

Additionally, it was found that the element having large neutron capture cross section such as Ir, can be precisely measured.

REFERENCES:

[1] R.Greenberg, P. Bode, E. De Nardi Fernandes, Spectrochim. Acta B, 66 (2011) 193-241.
[2] T. Miura, K.Chiba, T. Kuroiwa, T. Narukawa, A.Hioki,Matsue, Talanta, 82 (2010) 1143-1148.
[3] T. Miura, H. Matsue, T. Kuroiwa, J. Radioanal. Nucl. Chem., 282, 49-52, 2009.
[4] T. Miura, R. Okumura, Y. Iinuma, S. Sekimoto, K. Takamiya, M. Ohata, A.Hioki, J. Radioanal. Nucl. Chem., 303, 1417-1420, 2015.

CO12-12 Neutron Activation Analysis of Household Al foils in Chemical Experimental Class for Undergraduate Students

Y. Oura and N. Shirai

Graduate School of Science, Tokyo Metropolitan University

INTRODUCTION: Chemical experimental class is very important for undergraduate students in every department of chemistry in university. Third-year undergraduate students in department of chemistry, Tokyo Metropolitan University (TMU), perform instrumental analysis as well as traditional and fundamental gravitational analysis, volumetric analysis, and colorimetric analysis in the experimental class for analytical chemistry. And they determine Fe concentration in a household Al foil by three different analytical methods; colorimetric analysis, ICP atomic emission analysis (ICP-AES) and instrumental neutron activation analysis (INAA). After Fukushima accident in 2011, INAA have not been performed because of nonoperation of JRR-3, Japan Atomic Energy Agency. In 2018 INAA experiment have been opened again using Kyoto University Reactor (KUR).

EXPERIMENTS: Al foils in double polyethylene bags were irradiated together with known amount of Fe and Sc standard samples by neutrons for 2 hours in Pn-2 at KUR. Gamma-rays were measured for about 3 hours at the RI research facility, TMU.

A pair of students prepared an Al foil sample (about 12 mg) to be irradiated, then we performed neutron irradiation and gamma-ray measurement. Count values at channels around interested peaks and net peak areas calculated by Hypermet-PC software for Fe and Sc standard samples were given to students. We gave them a lecture about a gamma-ray spectrum and a way to calculate manually a peak area from the channel - count numerical data. They plotted gamma-ray spectra, fixed channel regions for background and gamma-ray peak, and calculated Fe and Sc concentrations in Al foil using 2 different gamma-ray each (1099 keV and 1292 keV for Fe (^{59}Fe), and 889 keV and 1112 keV for Sc (^{46}Sc)).

RESULTS: 24 Al samples of different 16 products were totally analyzed. Determined concentration values of Fe using 1099 keV and 1192 keV gamma-ray were varied from 0.52 % to 1.2 % and from 0.50 % to 1.3 %, respectively. All students obtained consistent Fe concentrations for two different gamma-rays. For Sc, two determination values using 889 keV and 1121 keV gamma-ray were varied from 0.013 ppm to 0.096 ppm and 0.020 ppm to 0.078 ppm, respectively. Because of a smaller count (about 100 counts) consistency between two determination values for Sc was poorer than for Fe. Since 1115 keV gamma-ray of ^{65}Zn was appeared near 1121 keV gamma-ray of ^{46}Sc, some students calculated Sc concentration using gamma-ray of ^{65}Zn instead of ^{46}Sc or a background region included gamma-ray of ^{65}Zn for calculating a net area of 1121 keV gamma-ray. They reported different Sc concentrations between two gamma-rays, although we talked in the class that concentrations using each gamma-rays should be almost same.

Fe in Al foil was also determined by colorimetric analysis and ICP-AES in the class. About 200 mg of Al foil was dissolved in HCl then this solution was used for both analytical methods. Determination values by colorimetric analysis tend to be systematically smaller than ones by ICP-AES for many students. And determination values by ICP-AES were systematically larger than ones by INAA in 2018. We have no idea for a reason of this systematic higher Fe concentration by ICP-AES at present. One possible reason is inaccuracy of concentrations of Fe standard solutions used for three analytical methods, which were prepared for each method. Comparison between determination values by INAA and ICP-AES is shown in Fig.1 A variation of values by INAA is obviously smaller than by ICP-AES, though values by INAA are systematically smaller. It means generally that even beginners determine easily and appropriately by non-destructive INAA, which does not need chemical processes. In ICP-AES, quite a lot of nonlinear standard addition calibration curves were reported because of assumable inaccurate pipetting for adding standard solution.

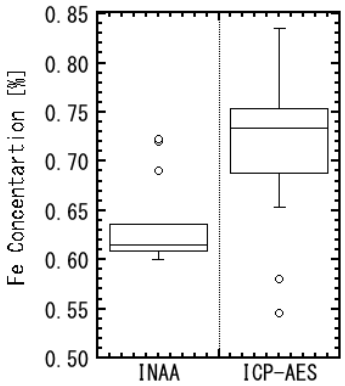

Fig. 1. Fe concentrations in Al foils of a manufacture determined by INAA and ICP-AES.

Concerned matter for INAA as an experimental class is that if KUR operates during when a class is open. In 2018 KUR started running after normal period of the class. We were anxious about the time schedule. This is an impenetrable difficulty.

CO12-13 Neutron induced prompt gamma ray measurement for nuclear power monitoring

K. Okada, A. Fushimi, S. Sekimoto[1] and T. Ohtsuki[1]

Center for Technology Innovation – Energy, Research and Development Group, Hitachi, Ltd.

[1] *Institute for Integrated Radiation and Nuclear Science, Kyoto University*

INTRODUCTION: Nuclear reactor power is monitored using neutron detectors in boiling water reactors (BWRs). Conventionally, fission chambers are adopted as the neutron detectors. Four fission chambers are installed as a single instrumentation tube and measure the local power at specific positions in the tube. As the fission chambers are located inside the reactor core of a reactor pressure vessel (RPV), maintenance of the chambers is difficult because the radiation dose rate of the area is high even during periodical inspection.

We considered a method in which the detector is located outside the RPV by converting neutrons into prompt gamma rays by a neutron capture reaction. Four kinds of metal boards are placed in neutron flux monitoring positions inside an instrumentation tube. Prompt gamma rays are emitted by neutron capture reactions between the metals and the neutrons. The gamma rays are measured by a gamma ray spectrometer located outside the RPV. The energy distribution of the gamma rays is specific for each metal, and their intensity is proportional to the thermal neutron flux at the position of each metal board. Therefore, the thermal neutron flux at each board position can be monitored by measuring the prompt gamma rays as the count rate of each gamma ray emission. By using this method, no detectors need to be installed in the reactor core.

In this study, we considered the identification of the peaks in an assumed situation where prompt gamma rays were emitted from four different metals at the same time. We confirmed that at least one peak for each of the four candidate metals was able to be separated from the peaks derived from the other candidate metals.

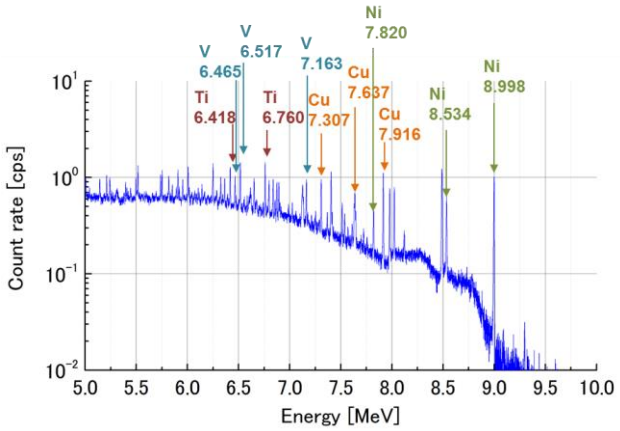

Figure 1: Energy spectrum which was obtained by superposing four energy spectra of the candidate metals

EXPERIMENTS: We limited the measurement energy to be above 5 MeV. Environmental gamma rays including decay gamma rays from radiated materials and scattered gamma rays mainly have an energy less than 3 MeV. When a high energy gamma ray is detected, a double escape peak is seen in the energy spectrum. The double escape peak is a peak having an energy 1.022 MeV lower than the energy of the gamma ray entering the detector. Thus, the lower energy limit of 6 MeV for the emitted prompt gamma ray was determined for separation of prompt gamma rays from environmental gamma rays in the energy spectrum. We chose Ti, V, Ni, and Cu as candidate metals by evaluating the prompt gamma ray emission rates estimated using nuclear data [1, 2].

We conducted a thermal neutron irradiation experiment for the candidate metals in the B4 port of the Kyoto University Research Reactor. The irradiation neutron flux to the candidate metals was 10^7 $cm^{-2}s^{-1}$. The thermal neutron beam size was 1 cm in width and 7 cm in height. The detector was a HPGe detector with relative efficiency of 33.4%. The surface of each piece of the target metals was larger than that of the thermal neutron beam.

RESULTS: We obtained four energy spectra above 5 MeV for the candidate metals. Figure 1 shows the energy spectrum which was obtained by superposing the four energy spectra. Labeled energies are full energy peaks separated from the peaks derived from the other candidate metals. The peaks which are not labeled were mainly escape peaks.

More than two peaks for each of the four candidate metals were identified. Thus, we confirmed that at least one peak for each of the four candidate metals was able to be separated from the peaks derived from the other candidate metals by using the HPGe detector.

REFERENCES:

[1] H. D. Choi, R. B. Lindstrom, G. L. Molnár Molnár, S. F. Mughabghab, R. Paviotti-Corcuera, Z. Révay, A. Trkov, V. Zerkin and C. Zhou, International Atomic Energy Agency, STI/PUB/1263 (2007) 87-194.

[2] Z. Révay, R. B. Firestone, T. Belgya and G. L. Molnár, G. L. Molnár (ed), Kluwer Academic Publishers, Dordrecht/Boston/New York (2004) 173-364.

CO12-14 **Beam Test of a micro-cell MWPC for a muon-electron conversion search experiment, DeeMe**

M. Aoki, N. Abe[1], M. Adachi[2], T. Hori, D. Nagao, H. Natori[3], T.M. Nguyen[4], R. Nishikawa, Y. Seiya[2], T. Takahashi[1], T. Takahashi[2], N. Teshima[2], K. Yamamoto[2] and H. Yoshinaka[2]

School of Science, Osaka University
[1] KURN, Kyoto University
[2]Faculty of Science, Osaka City University
[3]Institute for Basic Science, Korea
[4]University of Science and Technology Da Nang City

INTRODUCTION: There has been no observations related to a charged-lepton flavor violation (CLFV) process such as $\mu \to e\gamma$, μ-e conversion, τ-CLFV decays and so on. Based on this fact, the charged-lepton flavor is assumed to be conserved a priori in the Standard Model of particle physics (SM). However, it is rather natural not to be conserved in most of the models beyond SM (BSM). Any discoveries or improvements of the upper limit on the branching ratio of CLFV processes provide very important information to BSM. DeeMe is one of experiments that aim to search for CLFV with μ-e conversion in nuclear field [1]. It uses high-power high-purity pulsed proton beam from J-PARC RCS. The detector of DeeMe should be operational after $\mathcal{O}(\mu s)$ from a burst of particles (100 GHz/mm^2). We successfully developed such a detector with high-voltage switching technique [2]. It is very important to evaluate the performance of the detector before we start the physics data taking at J-PARC MLF.

EXPERIMENTS: The experiments were performed in 2 steps. In the 1st measurement, a gas mixture of the detector (Multi-Wire Proportional Chamber, MWPC) was optimized so that the delayed false pulses were suppressed while the gas gain was retained. A prototype MWPC was placed at the end of the beam line in the target room of the electron LINAC facility, and the waveforms from the readout strips were recorded with several different gas mixtures by using a special FADC system [3]. The several different sets of gas mixtures with small amount of SF_6 (0.05%, 0.1% and 0.15%) resulted in substantial drops of the detection efficiency. The gas mixture with 6% of R134a showed good efficiency and suppression on the delayed false pulses.

In the 2nd measurement, three MWPCs were sequentially placed so that the beam electrons hit through all three of them. The gas mixture was the one with R134a that provided less delayed false pulses.

At first, the low rate electron beam was used and the difference between the hit position at the 2nd MWPC from the expected hit position calculated with the 1st and 3rd MWPCs was evaluated. Figure 1 shows the typical distribution of the position difference. The obtained positional resolution is good enough for the μ-e conversion measurement. Please note that it was under the influence of the multiple-scattering and the further analysis is necessary to derive the intrinsic MWPC resolution.

Secondly, the high rate burst beam was injected to the MWPCs, and the off-timing field-emission electrons were used to derive hit efficiency and the random coincidence from the false pulses after the burst. The analysis is still ongoing.

RESULTS: The mixture of SF_6 does not improve the MWPC total performance. The mixture of R134a suppresses the delayed false pulses without apparent efficiency drop, thus it is very promising. The optimal gas mixture shall be 74% Ar, 20% i-C4H10 and 6% R134a. Another quench gas such as Methylal instead of R134a will be tested in 2019.

The positional resolution of MWPC is good enough for the μ-e conversion measurement. The detailed analysis is ongoing.

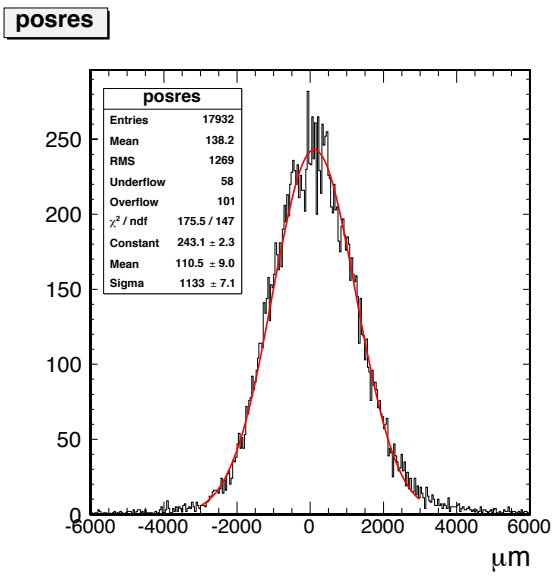

Fig. 1 A difference between the hit position of the 2nd MWPC from the expected hit position with the 1st and 3rd MWPCs.

REFERENCES:

[1] N. Teshima on behalf of the DeeMe Collaboration, "DeeMe experiment to search for muon to electron conversion at J-PARC MLF", in proceedings of NUFACT conference PoS (NuFact2017) 109 (2018).
[2] H. Natori, *et al*., "A fast high-voltage switching multi-wire proportional chamber", Prog. Theor. Exp. Phys. 2017(2) 023C01 (2017).
[3] N.M. Truong, *et al*., "Real-Time Lossless Compression of Waveforms Using an FPGA", IEEE Trans. Nucl. Sci. 65 2650 (2018).

CO12-15 Research on activation assessment of a reactor structural materials for decommissioning

M. Seki, K. Ishikawa, H. Nagata, K. Ohtsuka, T. Ohmori, H. Hanakawa, H. Ide, K. Tsuchiya, T. Sano[1], Y. Fujihara[1], J. Zhang[1] and J. Hori[1]

Department of JMTR, Japan Atomic Energy Agency [1]KURNS, Kyoto University

INTRODUCTION: JMTR (Japan Materials Testing Reactor) was decided as a decommissioning facility in the medium- and long-term plan of JAEA published in April 2017. Radioactive wastes are stored in drums and filled with concrete. However, since metal aluminum reacts with an alkaline substance such as concrete to generate hydrogen gas, there is a possibility that the manufactured waste packages may be damaged. Therefore, the treatment technology for radioactive aluminum waste has not been established, and it is stored in the plant.

The process of forming aluminum hydroxide ($Al(OH)_3$) via aluminate when metal aluminum is dis-solved with a strong base is known[1],[2]. It is converted to stable aluminum oxide (Al_2O_3) using this reaction. In cold tests, impurities were understood that it was in-dissolubility in sodium hydroxide (NaOH) in A6061 of Al-Mg-Si based materials but it was unknown to a de-tailed element.

This report was intended to recognize the behavior of impurities included within the aluminum alloy from an activation analysis.

EXPERIMENTS: The aluminum samples were ir-radiated in Pn-2 of KUR and cooled for 4 days. Table 1 shows the irradiation conditions of test samples in Pn-2 and Table 2 shows the chemical compositions of test samples. After irradiation, each sample was dissolved in a NaOH solution to form sodium aluminate ($Na[Al(OH)_4]$). A hydrochloric acid solution was added to the $Na[Al(OH)_4]$ solution for neutralization to pre-cipitate and to recover as $Al(OH)_3$ by the reaction of Equations (1) and (2). The radioactivity of the obtained materials in each process was measured using the gamma ray spectrometer.

$$2Al + 2NaOH + 6H_2O \rightarrow 2Na[Al(OH)_4] + 3H_2 \quad (1)$$

$$Na[Al(OH)_4] + HCl \rightarrow Al(OH)_3 + NaCl + H_2O \quad (2)$$

RESULTS and DISCUSSIONS: Table 3 shows the results of radioactivity measurement of aluminum samples, solids recovered in the filter and solutions after the filtration. The impurities such as ^{51}Cr and ^{59}Fe contained in each aluminum sample were not dis-solved in NaOH and remained as residuals, so they were separated by filtration.

^{24}Na was detected in the solution after filtration and was not recovered as the solid in the filter. ^{24}Na is generated by the reaction of fast neutrons ($^{27}Al(n, \alpha)\ ^{24}Na$). Thus, it is assumed that $^{24}Na[Al(OH)_4]$ has the same chemical behavior as Na^+ ion (see Eq.(1)).

$^{24}NaCl$ will be produced by the neutralization and collected with $Al(OH)_3$ (see Eq.(2)). Actually, it has been found that NaCl is contained in the gel of $Al(OH)_3$ in the test with the un-irradiated aluminum samples. It seems that $^{24}NaCl$ is able to be removed from the re-covered $Al(OH)_3$ by the washing with water after dry-ing and grinding if it is necessary to reduce the radio-activity of the wastes after treatment.

Table 1 Irradiation conditions of test samples in Pn-2.

Items	Values
Thermal power Thermal	5 MW
neutron flux Epithermal	2.8×10^{17} $m^{-2}s^{-1}$
neutron flux Fast neutron	1.1×10^{16} $m^{-2}s^{-1}$
flux Irradiation time	6.0×10^{16} $m^{-2}s^{-1}$
Cooling time	20 min.
Sample	4 days
	0.5 g

Table 2 Chemical Compositions of test samples

Element	A1050	A6061
Si	0.07	0.61
Fe	0.34	0.42
Cu	0.01	0.28
Mn	0.00	0.02
Mg	0.00	0.99
Cr	-	0.24
Zn	0.00	0.01
Ti	0.02	0.04
V	0.01	-0.01
other	0.00	
Al	99.54	97.92

Table 3 Main radioactive elements in each process

	Aluminum sample [Bq]	Recovered solid [Bq]	Solution after filtra-tion [Bq]
A1050			
^{54}Mn	2.81×10^{3}	7.66	1.78×10^{2}
^{59}Fe	1.74×10^{2}	1.64×10^{2}	-
^{24}Na	3.69×10^{5}	-	2.90×10^{5}
A6061			
^{51}Cr	3.64×10^{4}	3.77×10^{4}	3.80×10^{2}
^{54}Mn	1.91×10^{3}	1.63×10^{1}	4.22×10^{1}
^{59}Fe	2.25×10^{2}	1.95×10^{2}	-
^{24}Na	3.39×10^{5}	-	2.57×10^{5}

Remarks) No correction of measured values by the sample shapes in this test.

CONCLUSION: The preliminary test for the stable treatment of radioactive aluminum was performed by the wet process. The radioactive elements such as ^{51}Cr and ^{59}Fe in the aluminum alloys are able to be removed by this treatment and ^{24}Na will be reduced in the treatment process. In future, the optimization tests will be carried out for the production of the stable Al_2O_3.

REFERENCES:

[1] Taichi Sato, Journal of the Mineralogical Society of Japan, 19(1), 1989, pp.21-41.

[2] Gitzen, W.H. (ed.), *Alumina as a ceramic material*., American Ceramic Society, 1970.